

Article

# The Locking Depth of the Cholame Section of the San Andreas Fault from ERS2-Envisat InSAR

Guillaume Bacques, Marcello de Michele \*, Daniel Raucoules  and Hideo Aochi

BRGM, French Geological Survey, 3 avenue Claude Guillemin, 45100 Orléans, France; guillaumebacques@gmail.com (G.B.); d.raucoules@brgm.fr (D.R.); h.aochi@brgm.fr (H.A.)

\* Correspondence: m.demichele@brgm.fr

Received: 29 June 2018; Accepted: 2 August 2018; Published: 7 August 2018



**Abstract:** The Cholame section of the San Andreas Fault (SAF), which has been considered locked since 1857, has been little studied using geodetic methods. In this study, we propose to use Interferometric Synthetic Aperture Radar (InSAR) to contribute to the improvement of the knowledge of this section of the SAF. In particular, the objective of this work is to provide a description of the transition between the Parkfield and Cholame-Carrizo segments further southeast by producing an estimate of the locking depth of the Cholame segment by combining ERS2 (European Remote Sensing) and Envisat Advanced SAR (ASAR) satellites data. Our results indicate that the locking depth between the Parkfield and the Cholame-Carrizo segments deepens to the southeast. We then use these results as a hint to refine the tectonic loading on this section of the SAF.

**Keywords:** San Andreas Fault; Cholame section; Parkfield section; InSAR; ERS; Envisat; tectonic

## 1. Introduction

The Pacific Plate moves relative to the North American Plate at 3.5 cm/year. This displacement is partly accommodated at the borders of the two plates by strong earthquakes, partly through aseismic creep. This dextral strike-slip fault crosses the state of California (USA) over 1100 km from the Gulf of California in the south to Mendocino in the north. The San Andreas Fault (SAF) is locked for most of its length, except for its central part in continuous slip, e.g. Titus et al. [1]. It is responsible for strong earthquakes, some of which have marked the history of the United States of America (Fort Tejon 1857, San Francisco 1906, Long Beach 1933, County Kern 1952, Loma Prieta 1989).

At the transition between the southern limit of the portion of the San Andreas Fault in continuous slip (25–30 mm/year) [1–5] and the Cholame and Carrizo sections (that broke in 1857) lies the Parkfield section (Figure 1). The Cholame-Carrizo section is positioned about 20 km southeast of the 2004 Parkfield earthquake epicenter (Figure 1).

Most of the studies dealing with the Creeping, Parkfield, and Cholame sections of the SAF rely on the assimilation of both local and regional data to give a broad view of the fault behaviour at depth. The mechanisms responsible for fault relaxation are still difficult to define, and are the subject of discussions. They range from postseismic slip (following the 28 September Mw6 Parkfield earthquake—PKEQ) composed essentially of afterslip to postseismic slip that would be a mixture of several mechanisms (essentially afterslip and viscoelastic relaxation). For example, on the basis of analysis of Global Positioning System (GPS) and a creepmeters time series, Johanson et al. (2006) [6], Freed (2007) [7], and Barbot et al. (2008, 2013) [8,9] showed that fault motion after the PKEQ is essentially due to afterslip at least for the first two years following the earthquake. However, Johnson et al. (2006) [6] underlined the possible presence of other mechanisms that could explain the deformations recorded by GPS in the longer term. In this respect, Freed (2007) [7] estimated that the stress variation caused by the PKEQ is not sufficient to have solicited the lower part of the brittle crust and the upper

part of the mantle, and therefore it is unlikely that the earthquake caused viscoelastic relaxation. In a more recent study, Bruhat et al. (2011) [10] showed that it is nevertheless necessary to introduce deep viscoelastic slip (between 20–26 km deep) in order to explain the temporal evolution of GPS in the far field over the first five years following the PKEQ. They estimate that viscoelastic mechanisms contribute about 20% of the total movement measured by GPS in the far field and nearly 5% of the displacement for a GPS located in the near field. Thus, fault behaviour at depth following the 2004 Parkfield earthquake remains subject to discussion.

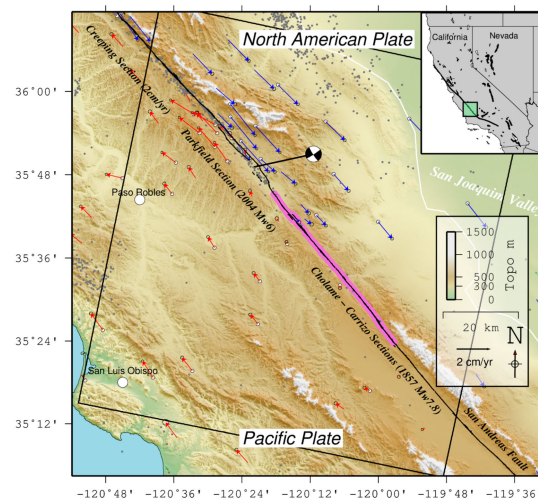


**Figure 1.** Location map and tectonic context. The right lateral strike-slip San Andreas Fault (SAF) trace as well as the Synthetic Aperture Radar (SAR) image acquisition geometry are presented by the black central line and the black square, respectively. The SAR presented track is the n°256, frame 2889, polarisation VV, C band. The Cholame section of the SAF is underlined in purple. The seismicity activity between 2005–2010 is presented as dark gray dots. The focal mechanism of the 2004 Mw6 Parkfield earthquake is presented. The blue and red arrows present the relative horizontal velocity between the North American Plate and the Pacific Plate recorded by the permanent GPS stations of the Central California Network between 2005–2010. The numerical elevation model is derived from the SRTM (Shuttle Radar Topography Mission).

Few studies have concentrated on the characterisation of the transition between the Parkfield segment and the Cholame-Carrizo segment of the SAF. Broadly, this transition is considered as a sharp changing rheology: slip-to-locked. Nevertheless, spatially detailed studies based on InSAR have suggested surface fault motion between the Parkfield section and the Cholame-Carrizo section, which was previously unconsidered in the modelling of the SAF behaviour at depth [4,11]. According to these studies, the velocity transition would be smoother than originally thought, thus calling for a re-thinking of the slip deficit in the area. In this study, we focus on a particular, local-scale area. We concentrate on the transition between the Parkfield segment and the Cholame-Carrizo segment after the 2004 Parkfield earthquake. Our approach estimates a preliminary and first-order characterisation of this particular transition, particularly the locking depth and the slip velocity at depth, which are important information that, at the time of writing, do not appear to have been documented since 1988 [12].

## 2. Materials and Methods

To achieve our objectives, we used the InSAR measurements obtained in a previous work [11] where we applied a stepwise stacking approach to produce a time series of surface displacement between 2005–2010 along the Creeping, Parkfield, and Cholame-Carrizo sections of the SAF. For the aims of the present study, we only exploit the full stack between 2005–2010 presented in

Bacques et al. [11] (Figure 2). We recall here the basic processing principles used in this previous study; we invite the reader to refer to Bacques et al. [11] for more details about the data source.

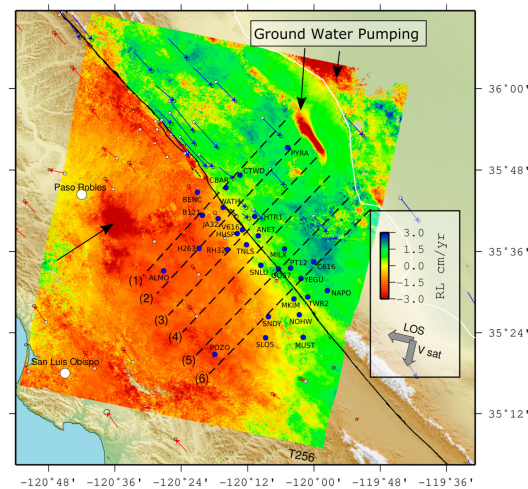


**Figure 2.** The 2005–2010 interferograms stack used in this study, the across-fault profiles (numbered from 1 to 6, dashed lines) at the location of the Cholame section of the San Andreas Fault and the SGPS network stations, locations, and names (blue circles) are presented here. The stack is composed by 43 interferograms computed from images acquired by Envisat-ASAR and ERS2 between 2005–2010. The color scale gives the deformation velocity in fault right lateral geometry (RL). The ground deformations due to water pumping (or oil extraction) are indicated by black arrows (Paso Robles, Coalinga, San Joaquin Valley).

### 2.1. InSAR Data Processing

As a reminder, the Synthetic Aperture Radar (SAR) dataset consists of 37 ERS2 and 24 Envisat ASAR raw images acquired between 2005–2010 (see Figure 1; track 256, frame 2889, descending mode, C-band, VV polarisation, Envisat i2 mode). We processed the SAR data and produced differential interferograms using the GAMMA software. We focused each image with an individual estimate of Doppler parameters. We then co-registered our entire dataset to a single reference image (Envisat) and calculated the interferograms separately for ERS2 and Envisat. After the reduction of the topographic contribution to the interferometric phase, we unwrapped each interferogram using the minimum cost flow method [13]. It is possible to reduce the errors of unwrapping by setting a interferometric signal coherence threshold below which the unwrapping is not carried out. According to our experiences and preliminary tests, we set this threshold at 0.4. Then, we subsampled the data by a factor of two in range and 10 in azimuth, and corrected the interferograms from the atmospheric effects. We initially obtained about 400 interferograms from both ERS2 and Envisat, among which we chose good signal coherence interferograms particularly close to the fault line. Low signal coherence is usually due to temporal changes in agricultural zones (e.g., the Cholame plain and the San Joaquin Valley). At the end of the processing, we kept 43 interferograms, including 20 from ERS2 and 23 from Envisat, which we merged in a stepwise stacking procedure.

### 2.2. Stacking

We produced five estimations of the ground displacement velocity according to five predefined periods: 2005, 2006–2007, 2008, 2009–2010, and 2005–2010. This allowed us to extract information on the kinematic of the SAF between 2005–2010 along the Parkfield section and the Cholame-Carrizo sections. In this study, for the sake of fault parameters retrieval through modelling of the Cholame section of the SAF, we are interested in the mean fault velocity at the location of the Cholame section. For this reason, we focused our attention on the stack of interferograms covering the 2005–2010 period

(Figure 2). This stack of 43 preselected ERS2-Envisat interferograms well suits the scope of this study. It maintains the advantage offered by the ERS2 and Envisat dual acquisition with no common dates. It is effective in terms of the conservation of the spatial resolution ( $50 \text{ m} \times 50 \text{ m}$ ) and the minimisation of atmospheric bias, and thus presents a satisfying signal-to-noise ratio. This stack is finally adjusted to the GPS values of the permanent stations of the central California GPS network, and projected in fault parallel geometry (Figures 1 and 2).

### 2.3. GPS

The GPS data used in Bacques et al. [11] come from the central California network. We retrieved them from the United States Geological Survey (USGS) website. The GPS data presented in Figures 1 and 2 were used to fit the interferograms stack to the local tectonic velocity ramp, following the methodology presented in Bacques et al. [11]. We used the entire GPS network presented in Figure 1, including GPS stations far from the SAF, but covered by our 2005–2010 stack.

In the present study, we also used GPS measurement campaigns (central California SGPS Network) to complete the GPS data at the Cholame section (Figure 2). These SGPS data consist of punctual measurements of the surface displacement at specific locations of permanent ground station markers by the use of mobile GPS devices. Compared with permanent GPS stations, the SGPS derived time series are irregularly time sampled; consequently, larger error bars can affect the retrieved mean velocity of ground displacement from these data. However, these data densify the spatial distribution of measurements at the location of the Cholame-Carrizo sections. In this study, we consider that the ground displacement velocity signal derived from InSAR is essentially parallel to the SAF. Therefore, we converted the ground displacement velocity derived from the northeast-up components of the SPGS records into the SAR line of sight (LOS), and then projected the results into the fault-parallel geometry. The WATH station served as velocity reference (Figure 2).

### 2.4. Modelling: Slip Velocity at Depth and Locking Depth

The locking depth ( $D$ ) of an active fault as well as the slip velocity at depth ( $S$ ) are important parameters for the estimation of the slip deficit and the estimation of seismic hazard. In this study, we estimate  $S$  and  $D$  at the Cholame segment using an elastic half-space deformation model recalled by Savage and Burford [14] and illustrated in Figure 3. This model allows one to relate, in case of a strike-slip fault such as the SAF, the surface deformation velocity derived from geodetic methods to the locking depth and the slip velocity at depth (below  $D$ ) through the following formulation:

$$V(x) = S/\pi \arctan(x/D) \quad (1)$$

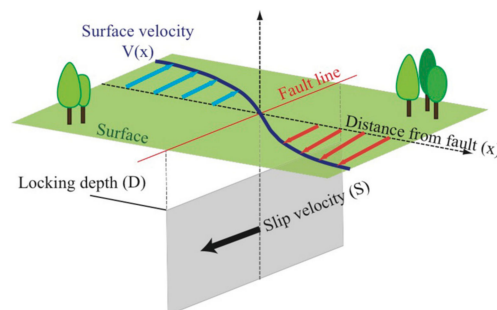


**Figure 3.** Illustration presenting the elastic dislocation model connecting the surface deformation  $V(x)$  to the locking depth ( $D$ ) as well as the slip velocity at depth ( $S$ ), which is illustrated here in the case of a dextral strike-slip fault.

Implicitly, the hypothesis that arises from this methodological choice is to consider that the Cholame section of the SAF does not undergo large lateral variations during the observation period. More precisely, this hypothesis consists in considering that throughout the period 2005–2010, the geometry of the surfaces locked on the fault plane (characterised by  $D$ ) and the velocities at depth (characterised by  $S$ ) are constant over time. This simplified hypothesis does not take into account the possible temporal evolution of the asperities of the Cholame segment, following the apparent relaxation of the Parkfield section throughout this period. However, in this work, we aim at estimating a first-order characterisation of the transition between the Parkfield and the Cholame sections of the SAF.

We extracted six profiles on the stack covering the period 2005–2010, crossing the fault line, and regularly spaced along the first 30 km from the southwestern boundary of the Parkfield segment at the location of the Cholame section (see Figures 1 and 2, the purple colored portion of the SAF). The extracted velocity profiles in the fault parallel geometry were centered on the intersection between the profile and the main fault line (Figure 4). Each InSAR profile is compared to the nearest SGPS ground station.

The model form has been adjusted to the InSAR profiles by varying the locking depth ( $D$ ) between 0–15 km (corresponding to the seismogenic zone of the SAF) as well as the slip velocity at depth ( $S$ ) between 0–10 cm/year, with steps of 0.1 km and 0.1 cm/year respectively. We did not include SGPS data in this inversion. For each pair of values ( $S$ ,  $D$ ), we have estimated the root mean square (RMS) of the residual between the corresponding profiles and the model that we want to adjust. This way, we determine the optimal torque ( $S$ ,  $D$ ) that minimises the RMS value (Figures 4 and 5). This approach, which is simple to implement, can be limited by the dispersion of the displacement velocity signal measured at the surface that results from non-tectonic phenomena (such as ground subsidence due to water/oil pumping, lower signal coherence level due to vegetation). Thus, it may happen that the couple ( $S$ ,  $D$ ) that minimise the RMS is not the most relevant one.

Therefore, we look for the solution that seems to be the most consistent for corresponding pairs of parameters ( $S$ ,  $D$ ).

As a reminder, the moment  $M_0$  (Nm) released by an earthquake breaking a fault segment is proportional to the total amount of fault slip ( $F_s$ ) times the total fault surface affected by the faulting ( $A$ ) times the elastic shear modulus of the earth crust ( $\mu = 33$  GPa) [15]:

$$M_0 = \mu F_s A \quad (2)$$

The magnitude of an earthquake ( $M_w$ ) is related to its moment ( $M_0$ ), in the International System of Units via [16–18]:

$$M_w = 2/3 \log_{10}(M_0) - 6 \quad (3)$$

Furthermore, in this work, starting from the ( $S$ ,  $D$ ) parameters we attempt to estimate the equivalent moment that would rise from a hypothetical earthquake that fully accommodates the slip deficit accumulated during the interseismic period. The slip deficit ( $F_s$ ) is defined as the product of the fault slip rate ( $S$ ) at depth and the time elapsed since the last earthquake ( $\Delta t$ ). The ruptured area ( $A$ ) is defined as the product of the length of the segment considered ( $L$ ) by the locking depth ( $D$ ). That is, from Equation (2) and the notation mentioned above, we can express this equivalent moment as follows (with  $F_s = S \Delta t$  and  $A = L D$ ):

$$M_0 = \mu S \Delta t L D \quad (4)$$

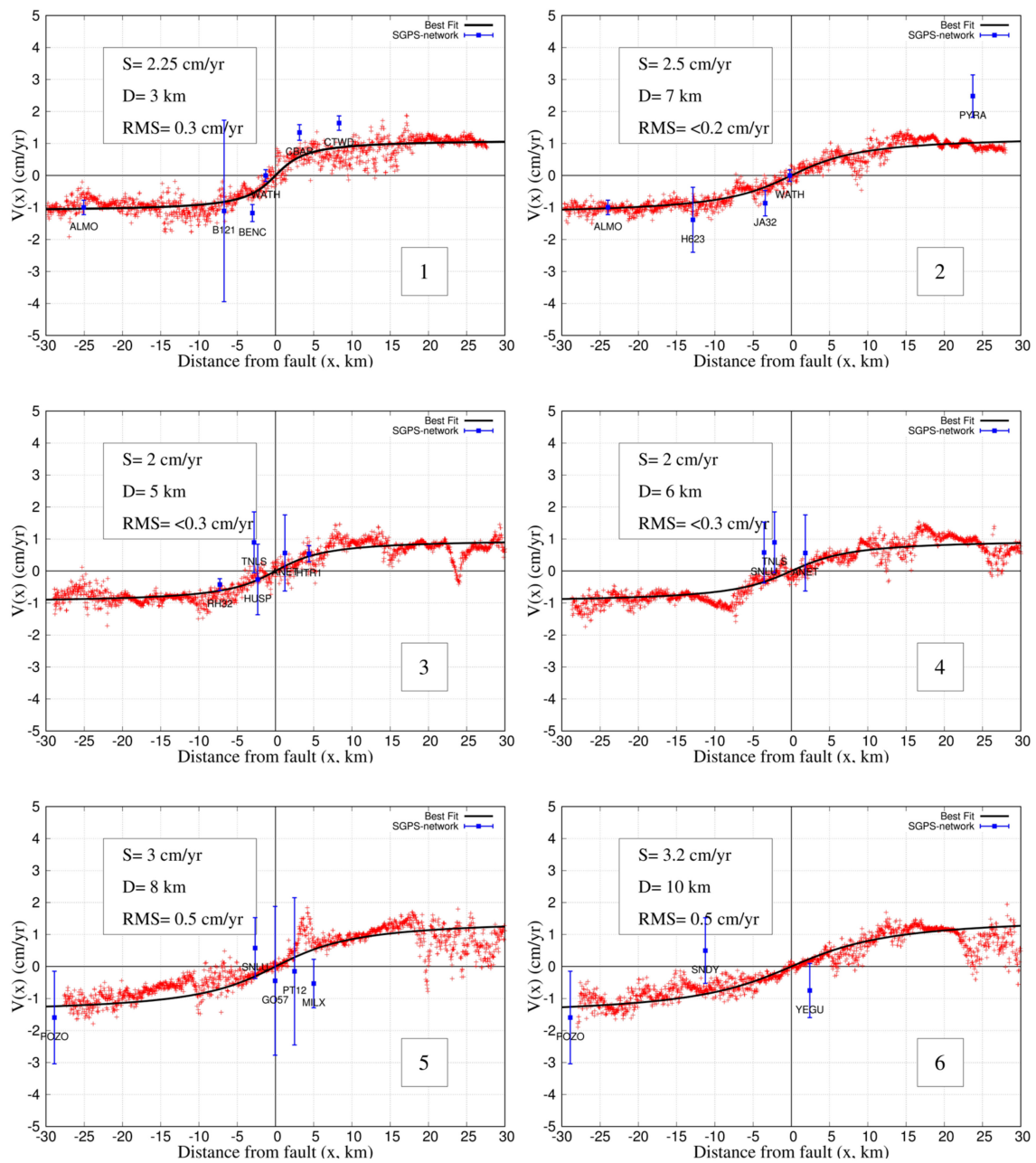


**Figure 4.** The surface deformation velocity profiles (cm/year) extracted across the Cholame segment (red points) according to the distance from the SAF (km). The black line represents the elastic dislocation model whose calibration parameters (slip velocity  $S$  and maximum locking depth  $D$ ) are recalled. SGPS-derived fault parallel velocities are also presented with the standard deviation as vertical error bars. The corresponding root mean square (RMS) between the presented model and the data is also recalled.

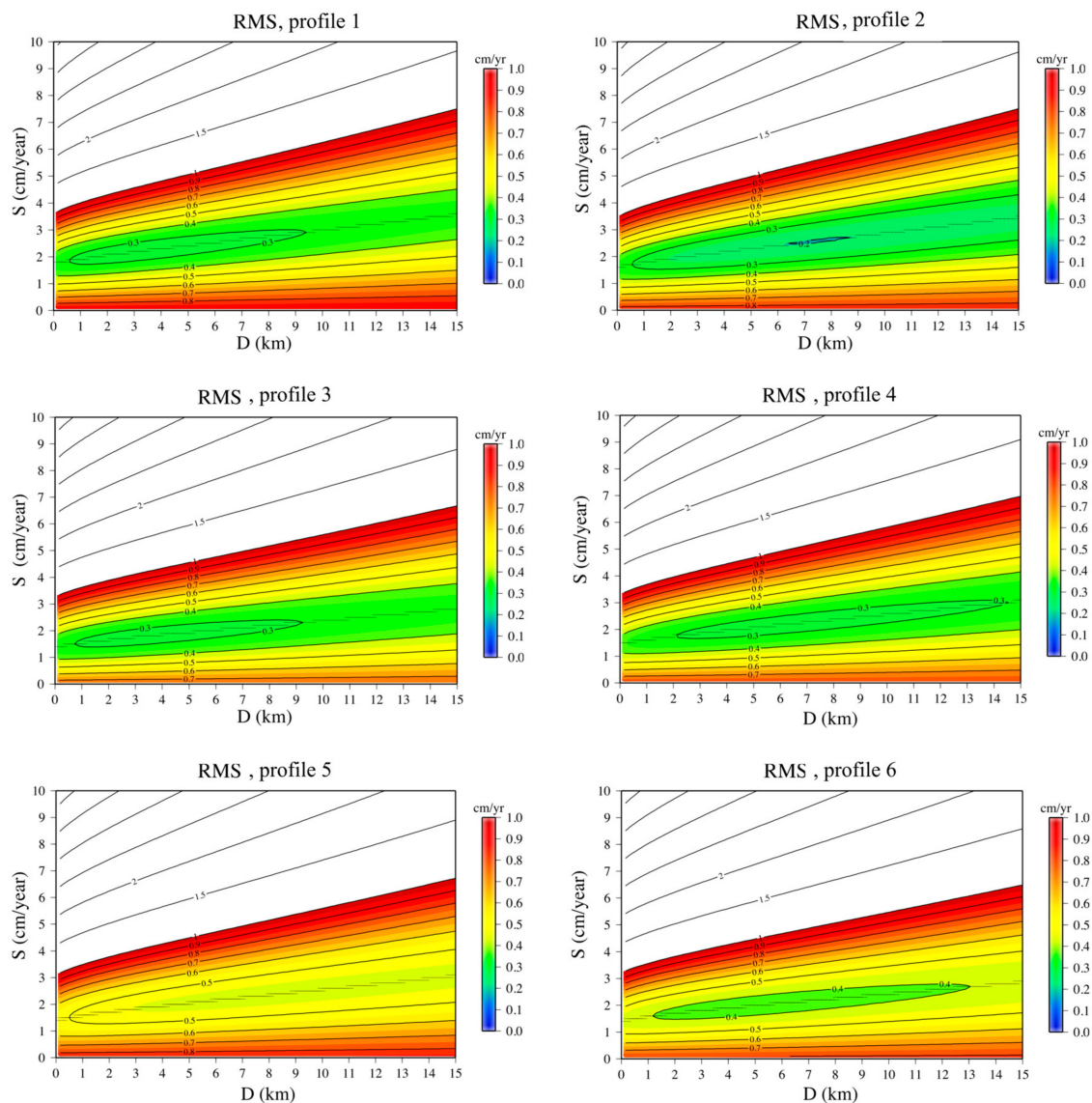


**Figure 5.** Estimation of the root mean square (RMS) of the residual between the data and the model parameterised by the locking depth ( $D$ ) and the slip velocity at depth ( $S$ ) for every profile (ranging from 1 to 6). The RMS is displayed in cm/year. The color code for the RMS is 0 cm/year (dark blue, perfect match) to 1 cm/year (red). The isolines are displayed every 0.1 cm/year between 0–1 cm/year, and then every 0.5 cm/year.

### 3. Results

From the stack of interferograms (Figure 2), we notice that the transition between the Parkfield section and the Cholame section of the SAF is very marked, reflecting a behavioural difference between these two sections, after the 2004 Mw6 Parkfield earthquake. In parallel, there is a clear distinction between the signatures of the Paso Robles subsidence and that of Coalinga (Figure 2), which is originated mainly from sediment compaction due to water pumping for the needs of agriculture, on the one hand, and for the extraction of oil, on the other hand. The image resolution shows that most of the surface displacement appears to be localised around the section of the SAF that broke in 2004, as well as the southeastern end of the creeping section. Moreover, we observe a decrease in the ground velocity as a function of the distance from northwest to southeast of the SAF, which corresponds to the increase in the depth of the seismicity as already observed in [4,11]). The transition between the Parkfield section and the Cholame-Carrizo section is the one that we focus on. The spatial

distribution of the SGPS measurements does not allow one to constrain the near-field evolution of the surface deformation rate across the fault line, particularly when looking at the profiles (3)–(6) (Figure 4). InSAR shows a improved spatial distribution of the interseismic deformation of the Cholame section of the SAF. It seems that the InSAR measurements have less dispersion than the SGPS measurements, such as for example the POZO, PT12, and B121 SGPS points.

The origin of this difference in accuracy between SGPS and InSAR could be due to different reasons. The GPS points are derived from measurement campaigns, and the estimation of the rate of deformation is based on few acquisition dates (sometimes simply two acquisitions spanned several years of interval). Thus, the velocities estimated can be affected by local and temporary phenomena such as zenith or tropospheric delay, which are seasonal effects that occurred at the time of the measurements. Meanwhile, the data from the InSAR came from a weighted average of several interferograms over nearly five years. Thus, although we have a good fit between SGPS and InSAR in the first and second profiles, it is possible that the SGPS measurements on the Cholame segment are less representative of interseismic displacement than the InSAR measurements. Nevertheless, not all InSAR profiles show the same level of dispersion. For example, the first profiles (1) between km 5–15, and the last two profiles (5) and (6) between km 20–30 show a significant variability in the velocity measurements (Figure 4). The origin of this variability can be attributed to the presence of crop fields (i.e., a loss of local signal coherence) or the important subsidence zone of San Joaquin Valley (Figures 1 and 2).

The fit of the arctangent deformation model via the D and S parameters (locking depth and slip velocity at depth, respectively) generally shows low RMS values (between 0.2–0.5 cm/year) although the corresponding solutions (S, D) are not unique (see Figure 5). We observe that the S value is better constrained for all of the profiles than the D value. However, the solutions proposed in the case of profile 2 (minimum RMS less than 0.2 cm/year, for D between 6–9 km) are also those that best correspond to the description of the InSAR profile. For the last two InSAR profiles (5) and (6), the method used seems to be very influenced by the greater variability of the signal between km 20–30. For these two profiles, the solutions chosen do not seem to correspond to low RMS solutions. The values of locking depth and slip velocity estimated for the rest of the profiles are summarised in Table 1.

**Table 1.** Presentation of the values S and D, extracted from the adjustment of the arctangent function for the ground surface velocity. The deficit slip, the RMS corresponding to the chosen solution as well as the equivalent seismic moment per 5 km of fault length determined from each pair (S, D) for each profile, are presented here.

Profile n°	1	2	3	4	5	6	Units
S	2.25	2.5	2	2	3	3.2	cm/year
D	3	7	5	6	8	10	km
Slip Deficit	347.5	385	308	308	462	493	cm
RMS	~0.3	<0.2	<0.3	~0.3	~0.5	~0.5	cm/year
$M_0$ (L = 5 km)	1.78	4.65	2.65	3.19	6.37	8.5	$\times 10^{18}$ Nm

Based on the parameters (S, D) chosen for each profile, the good fit between the model and the InSAR profiles suggests a relatively shallow locking depth (an average of nearly 7 km) with an average slip velocity between 2–3 cm/year. It appears that the locking depth increases as one moves along the Cholame segment from the northwest to southeast (Table 1). It reaches a depth of ~10 km at profile (6), with a slip velocity at depth at this location (3.2 cm/year) that is not too far from the slip velocity of the creeping segment (3.5 cm/year) and presents a good agreement with the study conducted by Harris and Archuleta [12] who estimate an average slip velocity of 3.6 cm/year for the Carrizo segment further southeast.

We pushed the exercise further; from the estimates of  $D$  and  $S$ , we calculated the slip deficit and the equivalent moment accumulated by this SAF segment since the last rupture of 1857. From each velocity–depth pair, we have estimated the amount of equivalent moments accumulated on the fault since the last rupture from 1857 to 2011 (154 years); the results are presented for each profile in Table 1. Roughly, if we consider the formulation presented by the equations mentioned above (3 and 4), and taking a fault length of 30 km for the Cholame section, an average value of the velocity at a depth of about 2.5 cm/year, and the time lapse since the last rupture, we obtain an equivalent moment of about  $2.78 \times 10^{19}$  Nm, or an equivalent magnitude ( $M_w$ ) of 6.9, with an associated cumulative slip of nearly 4 m at the surface.

#### 4. Discussions

In this study, we exploit the exceptional ground displacement generated by the fault motion after the 2004  $M_w$ 6 Parkfield earthquake, which is well detectable by SAR interferometry. We might not be able to perform this exercise before the period 2005–2010, as ground displacement at the study area was confined to a few mm per year, as shown in de Michele et al. [4].

The model used in this study is a simple elastic dislocation in a two-dimensional space under the assumption of a single fault. This dislocation model does not take into account the deep viscoelastic behaviours that, when considered, can reduce the locking depth. For example, Zielke et al. [18] estimate the locking depth at the Carrizo plain of about 20 km with slip velocity at depth of 3.8 cm/year with an elastic dislocation model, against a depth of 11 km with 4 cm/year using a viscoelastic model. Thus, our estimate of locking depth may be overestimated. However, we believe that the introduction of viscoelastic mechanisms less than 20 km deep is not a strong hypothesis. Indeed, at the depths considered in this study (less than 15 km) it seems more reasonable to think that the behaviour of the fault follows a rate and state friction law.

The Cholame section of the SAF covered by the first three profiles (1)–(3) presented a seismic activity over the period 2005–2010 whose distribution spreads between 6–14 km deep (e.g., Barbot et al. [8] Bacques et al. [11] which might indicates a segmentation of the fault frictional properties with depth at this location. From our measurements, the northwestern portion of the Cholame section exhibits an average locking depth of  $\sim 5$  km with an average slip velocity of 2.25 cm/year, which, taking into account the uncertainties, appears to be in good agreement with the segmentation with depth that is suggested by the seismicity distribution. Conversely, the portion of the Cholame section covered by profiles (4)–(6) had almost no seismicity over the first 15 km of depth. As for the northwestern portion of the Cholame section, the absence of seismicity suggests the a priori homogeneous behaviour of the fault over the first 15 km. However, the average locking depth of this portion of the SAF estimated in this study is  $\sim 8$  km, highlighting the depth dependence segmentation that does not appears to be revealed by the recorded seismicity. The progressive northwest–southeast increase in the locking depth (6–8–10 km) encourages the idea that this locked zone could extend towards the Carrizo section further to the southeast. The estimate average slip deficit of 4 m since 1857 seems consistent with the values reported by previous studies of paleoseismicity in this section of the SAF [19,20].

From these elements, it is difficult to assess with how much efficiency the fault accumulates elastic energy between 0–7 km depth, thus enabling the equivalent moment accumulation ( $\sim 2.78 \times 10^{19}$  Nm) since the last earthquake in 1857. Indeed, as an additional hint, in the work presented in Bacques et al. [11], we highlighted the presence of shallow transient surface creep along the 20 first km of the Cholame section (covering the first four profiles presented Figure 2) between 2005–2007. These transients are likely to affect the shallow portion of the fault with the consequence of reducing the effective locked area ( $A$ ) at this location, as assessed in this study. The use of more advanced modelling techniques [9,10], such as Okada-based methods, might give additional hints about the fault rheology along the transition Parkfield-Cholame-Carrizo of the SAF.

## 5. Conclusions

In conclusion, from the combination of ERS2 and Envisat SAR interferograms, we obtain a set of ground velocity profiles at a high spatial resolution. We concentrate on the transition between the Parkfield-Cholame-Carrizo sections of the SAF, which is traditionally considered a sharp creeping-to-locked transition. Using InSAR velocities and an elastic dislocation model, we make the following observations:

1. A progressive northwest–southeast increase in the locking depth (6–8–10 km) at the transition between the Parkfield-Cholame-Carrizo sections of the SAF.
2. An average locking depth of the Cholame segment is located at 7.5 km, with an average velocity at depth of nearly 2.3 cm/year.
3. If we consider the time interval between 1857–2011, this segment has a slip deficit of 4 m, which is in agreement with what has been documented using paleoseismicity on the Cholame and Carrizo sections of the SAF.

This shallow locking depth questions the effective elastic loading of this segment. More precisely, from this preliminary work, we can distinguish two zones of the Cholame section that present different fault properties: firstly, a northwest portion of Cholame section in the continuity of the Parkfield section over the first 20 km, which is thought to have low loading properties, and secondly, a more deeply locked zone in the southeast portion of the Cholame section, whose behaviour seems to be more similar to the Carrizo segment further southeast.

**Author Contributions:** Conceptualization, M.d.M., D.R. and H.A.; Formal analysis, G.B.; Investigation, G.B., M.d.M., D.R. and H.A.; Methodology, G.B., M.d.M. and D.R.; Supervision, M.d.M., D.R. and H.A.; Writing—original draft, G.B., M.d.M., D.R. and H.A.

**Funding:** This research was funded by the French Space Agency (CNES) and by the French Geological Survey (BRGM). We are thankful to the European Space Agency (ESA) for providing ERS and ENVISAT data at reproduction cost via a Cat. 1 project. The authors wish to thank Frédérique Rolandone for discussions.

**Conflicts of Interest:** The authors declare no conflict of interest.

## References

1. Titus, S.J.; DeMets, C.; Tikoff, B. Thirty-five-year creep rates for the creeping segment of the San Andreas Fault and the effect of the 2004 Parkfield earthquake: Constraints from alignment arrays, continuous global positioning system and creep-meters. *Bull. Seismol. Soc. Am.* **2006**, *96*, S250–S268. [[CrossRef](#)]
2. Rolandone, F.; Bürgmann, R.; Agnew, D.C.; Johanson, I.A.; Templeton, D.C.; d’Alessio, M.A.; Titus, S.J.; DeMets, C.; Tikoff, B. Aseismic slip and fault normal strain along the central creeping section of the San Andreas Fault. *Geophys. Res. Lett.* **2008**, *35*, L14305. [[CrossRef](#)]
3. Ryder, I.; Bürgmann, R. Spatial variations in slip deficit on the central San Andreas Fault from InSAR. *Geophys. J. Int.* **2008**, *175*, 837–852. [[CrossRef](#)]
4. De Michele, M.; Raucoules, D.; Rolandone, F.; Briole, P.; Salichon, J.; Lemoine, A.; Aochi, H. Spatiotemporal evolution of surface creep in the Parkfield region of the San Andreas fault (1993–2004) from Synthetic Aperture Radar. *Earth Planet. Sci. Lett.* **2011**, *308*, 141–150. [[CrossRef](#)]
5. Turner, R.C.; Shirzaei, M.; Nadeau, R.M.; Bürgmann, R. Slow and Go: Pulsing Slip Rates on the Creeping Section of the San Andreas Fault. *J. Geophys. Res. Solid Earth* **2015**, *120*, 5940–5951. [[CrossRef](#)]
6. Johanson, I.A.; Fielding, E.J.; Rolandone, F.; Bürgmann, R. Coseismic and postseismic slip of the 2004 Parkfield earthquake from space-geodetic data. *Bull. Seismol. Soc. Am.* **2006**, *96*, S269–S282. [[CrossRef](#)]
7. Freed, A.M. Afterslip (and only afterslip) following the 2004 Parkfield, California, earthquake. *Geophys. Res. Lett.* **2007**, *34*, L06312. [[CrossRef](#)]
8. Barbot, S.; Fialko, Y.; Bock, Y. Postseismic deformation due to the Mw 6.0 2004 Parkfield earthquake: Stress-driven creep on a fault with spatially variable rate-and-state friction parameters. *J. Geophys. Res.* **2009**, *114*, B07405. [[CrossRef](#)]

9. Barbot, S.; Agram, P.; de Michele, M. Change of apparent segmentation of the san andreas fault around parkfield from space geodetic observations across multiple periods. *J. Geophys. Res.* **2013**, *118*, 6311–6327. [[CrossRef](#)]
10. Bruhat, L.; Barbot, S.; Avouac, J.-P. Evidence for postseismic deformation of the lower crust following the 2004 mw 6.0 parkfield earthquake. *J. Geophys. Res.* **2011**, *116*. [[CrossRef](#)]
11. Bacques, G.; de Michele, M.; Raucoules, D.; Aochi, H.; Rolandone, F. Shallow deformation of the San Andreas fault 5 years following the 2004 Parkfield earthquake (Mw6) combining ERS2 and Envisat InSAR. *Sci. Rep.* **2018**, *8*, 6032. [[CrossRef](#)] [[PubMed](#)]
12. Harris, R.A.; Archuleta, R.J. Slip budget and potential for a m7 earthquake in central California. *Geophys. Res. Lett.* **1988**, *15*, 1215–1218. [[CrossRef](#)]
13. Costantini, M.; Rosen, P.A. A generalized phase unwrapping approach for sparse data. In Proceedings of the IEEE 1999 International Geoscience and Remote Sensing Symposium (IGARSS), Hamburg, Germany, 28 June–2 July 1999; Volume 1, pp. 267–269.
14. Savage, J.C.; Burford, R.O. Geodetic determination of relative plate motion in Central California. *J. Geophys. Res.* **1973**, *78*, 832–845. [[CrossRef](#)]
15. Kanamori, H. The energy release in great earthquakes. *J. Geophys. Res.* **1977**, *82*, 2981–2987. [[CrossRef](#)]
16. Hanks, T.; Kanamori, H. A moment-magnitude scale. *J. Geophys. Res.* **1979**, *84*, 2348–2352. [[CrossRef](#)]
17. Cavalié, O.; Lasserre, C.; Doin, M.-P.; Peltzer, G.; Sun, J.; Xu, X.; Shen, Z.-K. Measurement of interseismic strain across the Haiyuan fault (Gansu, China), by InSAR. *Earth Planet. Sci. Lett.* **2008**, *275*, 246–257. [[CrossRef](#)]
18. Smith-Konter, B.R.; Sandwell, D.T.; Shearer, P. Locking depths estimated from geodesy and seismology along the San Andreas Fault system: Implications for seismic moment release. *J. Geophys. Res.* **2011**, *116*, 12. [[CrossRef](#)]
19. Sieh, K.E. Slip along the San Andreas Fault associated with the great 1857 earthquake. *Bull. Sismol. Soc. Am.* **1978**, *68*, 1421–1448.
20. Zielke, O.; Arrowsmith, J.R.; Ludwig, L.G.; Akçiz, S.O. Slip in the 1857 and Earlier large Earthquakes along the Carrizo plain San Andreas Fault. *Science* **2010**, *327*, 1119–1122. [[CrossRef](#)] [[PubMed](#)]



© 2018 by the authors. Licensee MDPI, Basel, Switzerland. This article is an open access article distributed under the terms and conditions of the Creative Commons Attribution (CC BY) license (<http://creativecommons.org/licenses/by/4.0/>).